Discovery of Genes Essential for Heme Biosynthesis through Large-Scale Gene Expression Analysis

Roland Nilsson,[1,2,5,9] Iman J. Schultz,[3,4,9] Eric L. Pierce,[3,4] Kathleen A. Soltis,[3,4] Amornrat Naranuntarat,[6] Diane M. Ward,[7] Joshua M. Baughman,[1,2,5] Prasad N. Paradkar,[7] Paul D. Kingsley,[8] Valeria C. Culotta,[6] Jerry Kaplan,[7] James Palis,[8] Barry H. Paw,[3,4,*] and Vamsi K. Mootha[1,2,5,*]
[1]Department of Systems Biology
[2]Center for Human Genetic Research, Massachusetts General Hospital
[3]Department of Medicine, Hematology Division, Brigham and Women's Hospital
[4]Hematology-Oncology Division, Children's Hospital Boston
Harvard Medical School, Boston, MA 02115, USA
[5]Broad Institute of MIT/Harvard, Cambridge, MA 02142, USA
[6]Toxicology Division, Department of Environmental Health Sciences, The Johns Hopkins University Bloomberg School of Public Health, Baltimore, MD 21205, USA
[7]Department of Pathology, University of Utah School of Medicine, Salt Lake City, UT 84132, USA
[8]Department of Pediatrics, Center for Pediatric Biomedical Research, University of Rochester School of Medicine and Dentistry, Rochester, NY 14642, USA
[9]These authors contributed equally to this work
*Correspondence: bpaw@rics.bwh.harvard.edu (B.H.P.), vamsi@hms.harvard.edu (V.K.M.)
DOI 10.1016/j.cmet.2009.06.012

SUMMARY

Heme biosynthesis consists of a series of eight enzymatic reactions that originate in mitochondria and continue in the cytosol before returning to mitochondria. Although these core enzymes are well studied, additional mitochondrial transporters and regulatory factors are predicted to be required. To discover such unknown components, we utilized a large-scale computational screen to identify mitochondrial proteins whose transcripts consistently coexpress with the core machinery of heme biosynthesis. We identified *SLC25A39*, *SLC22A4*, and *TMEM14C*, which are putative mitochondrial transporters, as well as *C1orf69* and *ISCA1*, which are iron-sulfur cluster proteins. Targeted knockdowns of all five genes in zebrafish resulted in profound anemia without impacting erythroid lineage specification. Moreover, silencing of *Slc25a39* in murine erythroleukemia cells impaired iron incorporation into protoporphyrin IX, and vertebrate *Slc25a39* complemented an iron homeostasis defect in the orthologous yeast *mtm1Δ* deletion mutant. Our results advance the molecular understanding of heme biosynthesis and offer promising candidate genes for inherited anemias.

INTRODUCTION

Biosynthesis of heme is a tightly orchestrated process that occurs in all cells (Ponka, 1997). In most eukaryotes, heme synthesis (Figure 1A) is initiated in the mitochondrion by δ-aminolevulinic acid synthase (ALAS), which catalyzes the reaction between succinyl-CoA and glycine to form δ-aminolevulinic acid (ALA). ALA is exported to the cytosol, where it is converted through a series of reactions to coproporphyrinogen III. This molecule crosses the outer mitochondrial membrane, is oxidized by the CPOX enzyme in the intermembrane space, and is subsequently imported back into the mitochondrial matrix and further oxidized to protoporphyrin IX (PPIX). Heme synthesis is completed by the incorporation of ferrous iron into PPIX by ferrochelatase (FECH). Though these eight core enzymes have been extensively characterized, the means by which ALA and porphyrin intermediates enter the mitochondrion, how heme matures in the mitochondrion, and how it is then exported to the cytosol are largely unknown.

Heme serves as a prosthetic group in many enzymes that are involved in important processes such as electron transport, apoptosis, detoxification, protection against oxygen radicals, nitrogen monoxide synthesis, and oxygen transport (Ajioka et al., 2006). The latter process places a special demand for heme synthesis in the developing erythron, which needs to generate vast amounts of the oxygen carrier protein hemoglobin. In mammals, the regulation of heme synthesis differs between erythroid and nonerythroid cells. In nonerythroid cells, heme itself plays a key regulatory role and represses transcription through feedback mechanisms (May et al., 1995). In red blood cells, iron availability is the dominant factor (Ponka, 1997). Erythroid and nonerythroid cells also express distinct isoforms of the core heme biosynthesis enzymes. For example, the ubiquitous form of ALAS is encoded by *ALAS1*, whereas a separate gene *ALAS2* encodes the erythroid-specific enzyme. These different modes of regulation probably reflect the extraordinary need for mitochondrial iron assimilation and heme synthesis during erythroid maturation.

In recent years, several new genes involved in heme synthesis have been discovered. Genetic screening in zebrafish revealed that *Mitoferrin-1* (*SLC25A37*), a vertebrate homolog of the yeast mitochondrial iron importers *MRS3/MRS4*, plays an important
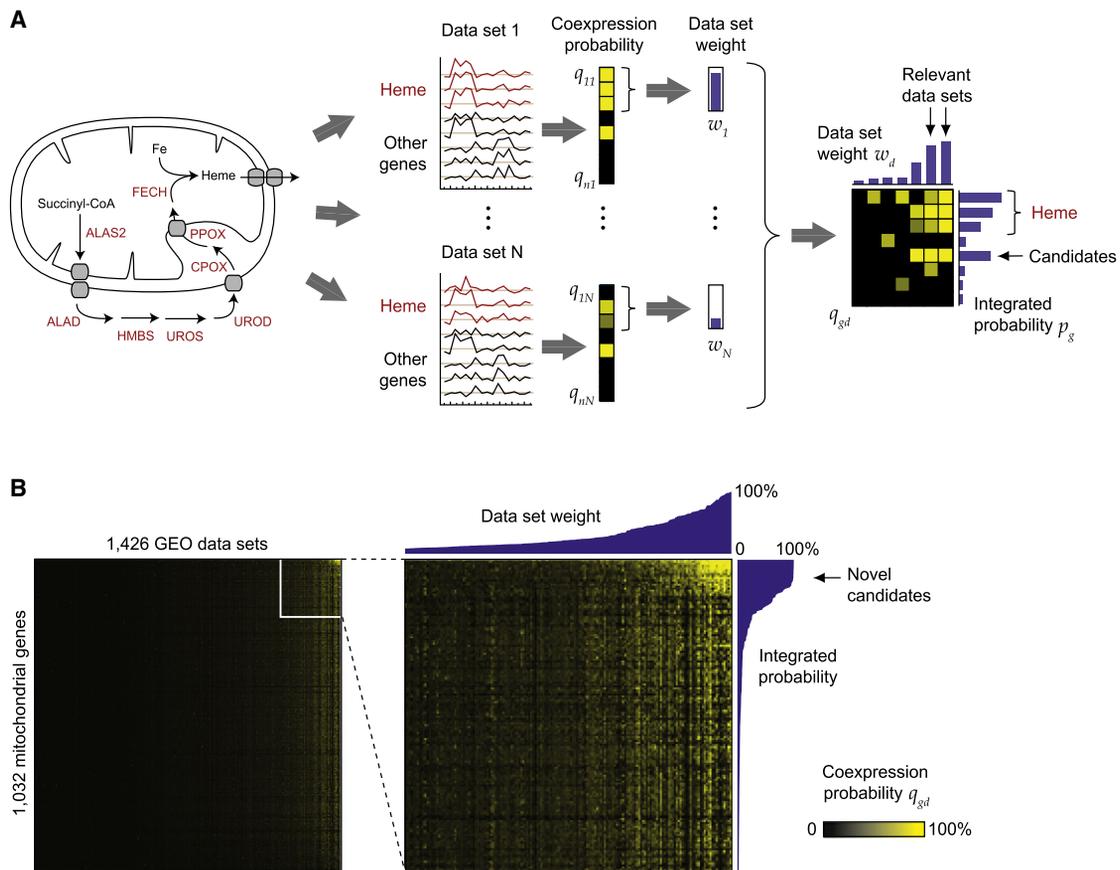
Figure 1. Identifying Candidate Genes for Heme Biosynthesis Using Expression Screening

(A) The eight known enzymes of heme biosynthesis pathway (left) define the query pathway. Using a rank-based statistic, each gene g is assigned a probability of coexpression q_{gd} in each microarray data set d (black/yellow columns). Data sets in which the heme biosynthesis enzymes are themselves tightly coexpressed are assigned larger weights w_d (blue vertical bars), which are then used to integrate the coexpression information from all data sets (black/yellow matrix, right) into a final probability p_g (blue horizontal bars).

(B) The coexpression matrix for the 1426 data sets used in this study (columns), over 1032 mitochondrial genes (rows). Yellow indicates strong coexpression. Right, a magnified portion of this matrix, with data set weights (top) and integrated probabilities (right).

role in heme metabolism in erythroid cells (Shaw et al., 2006a). A more ubiquitously expressed *SLC25A37* paralog, *SLC25A28*, is important for heme synthesis in nonerythroid cells (Paradkar et al., 2009; Shaw et al., 2006a). Unbiased functional screening methods have also, rather surprisingly, implicated genes involved in iron-sulfur (Fe-S) cluster synthesis as important for heme production. In yeast, deletions of several genes that are important for mitochondrial Fe-S cluster assembly negatively affect heme synthesis (Lange et al., 2004). Deletion of the mitochondrial ATP-binding cassette transporter *ABCB7*, which is an essential component of the Fe-S cluster export machinery, results in reduced heme levels in mouse erythrocytes (Pondarre et al., 2007). A study in the zebrafish mutant *shiraz* revealed that a mutation in the Fe-S cluster assembly gene glutaredoxin 5 (*GLRX5*) affects heme biosynthesis through the cytosolic iron responsive protein 1 (IRP1) (Wingert et al., 2005). Under low-iron conditions, diminished Fe-S cluster assembly induces IRP1 to lose its Fe-S cluster, resulting in binding to iron-responsive elements (IRE) and subsequent posttranslational regulation of genes involved in iron and heme homeostasis (Muckenthaler et al., 2008; Rouault, 2006). Wingert et al. showed that impaired

heme production in the zebrafish *shiraz* mutant was due to the constitutive repression of *ALAS2* by IRP1, thereby inhibiting *ALAS2* translation and subsequent production of heme. This study confirms the intimate relation between Fe-S cluster synthesis and heme biosynthesis (Lill and Mühlenhoff, 2008; Muckenthaler et al., 2008; Rouault, 2006).

Several human diseases have been linked to genes involved in heme biosynthesis. Mutations in any of the eight core enzymes except ALAS (Figure 1A) lead to various forms of porphyria (Sassa, 2006). Defects in *ALAS2*, *ABCB7*, *GLRX5*, and *SLC25A38* are each associated with different forms of sideroblastic anemias (Allikmets et al., 1999; Camaschella et al., 2007; Cotter et al., 1992; Guernsey et al., 2009), which are characterized by mitochondrial iron overload and impaired heme synthesis. Aberrant splicing of *SLC25A37* (Shaw et al., 2006b), deletion of IRP2 (Cooperman et al., 2005), and C-terminal deletions in ALAS2 (Whatley et al., 2008) are associated with a variant form of erythropoietic protoporphyria. Other human disorders involving defects in iron homeostasis and heme metabolism exist, and identifying the genes responsible is vital to understanding their nature and providing new ways for treatment.

Aiming to systematically identify new components of the heme biosynthesis pathway, we applied a computational screening algorithm that searches a large collection of microarray data sets for genes that are consistently and specifically coexpressed with the eight heme biosynthesis genes, depicted in Figure 1A. Applying this computational screening technique to a compendium of ~1100 mitochondrial genes yielded a collection of strong candidate genes. We used zebrafish as an in vivo vertebrate model system to test five high-scoring candidates. We found that all five genes are required for proper synthesis of hemoglobin, indicating high specificity of our computational predictions. We chose to study one candidate, the solute carrier *SLC25A39*, in greater detail in mouse and yeast, and our results support a role for this gene in maintaining mitochondrial iron homeostasis and regulating heme levels.

RESULTS

Using microarray technology, it is possible to measure the correlation of expression patterns on a whole-genome scale (Quackenbush, 2001). However, expression patterns may be correlated in a particular experiment for trivial reasons such as stress responses or adaptation to cell culture conditions (Cahan et al., 2007), so expression correlation does not in itself imply a close functional relationship. To address this problem and improve specificity, we reasoned that genes coexpressed consistently across many independent data sets, which interrogate different experimental conditions, are more likely to be functionally related. Based on this principle, we developed a computational technique that we call *expression screening* that integrates information from thousands of microarray data sets to discover genes that are specifically coexpressed with a given *query pathway*, such as mitochondrial heme biosynthesis (Figure 1A). We assembled a collection of 1426 mouse and human Affymetrix microarray datasets (~35,000 microarrays) representing a wide range of experimental conditions (see Experimental Procedures). For each data set in this collection, expression screening scores every gene for coexpression with the query pathway by using a rank-based statistic. Importantly, we also compute a measure of the intracorrelation of the query pathway in each data set, reflecting the extent to which the query pathway is transcriptionally regulated. Finally, we integrate the coexpression information from all data sets weighted by the query pathway intracorrelation. This weighting scheme allows the most "relevant" data sets to contribute the most to the final result and also permits the identification of biological contexts where the coexpression occurs.

A Large-Scale Computational Screen Reveals Genes Essential for Heme Biosynthesis

We applied expression screening to the eight well-characterized heme biosynthesis enzymes. Because proteins involved in heme biosynthesis are likely mitochondrial, we chose to limit our screen to a high-quality inventory of ~1100 nuclear genes encoding the mitochondrial proteome (Pagliarini et al., 2008). A fraction of these showed strong coexpression with the heme enzymes in a small number of data sets (Figure 1B). Among the top five coexpressed genes identified by our screen, not counting the heme biosynthesis enzymes themselves, four had previously been implicated in heme biosynthesis (Table 1). These were *ABCB6*, the only known transporter for a porphyrin intermediate (Krishnamurthy et al., 2006); *SLC25A37*, a mitochondrial solute carrier that supplies iron to mitochondria for heme and Fe/S biogenesis (Shaw et al., 2006a); *ABCB10*, which is induced by GATA1 during erythroid differentiation and enhances hemoglobinization (Shirihai et al., 2000); and *GLRX5*, which regulates heme synthesis through a feedback loop involving IRP1 (Wingert et al., 2005). At somewhat lower confidence levels, we found genes upregulated in red blood cells, reflecting the fact that erythropoiesis drives most of the coexpression signal for this pathway.

Several top-scoring candidates had not previously been implicated in heme biosynthesis or mitochondrial iron homeostasis. Because of the membrane transport events involved in heme synthesis (Figure 1A), we were particularly interested in orphan solute transporters. For follow-up studies, we selected three genes that we considered possible transporters: *TMEM14C*, a small transmembrane protein, and *SLC25A39* and *SLC22A4*, members of the solute carrier family. We also selected *ISCA1* (yeast *ISA1*) and *C1orf69* (yeast *IBA57*), which are known to participate in the maturation of Fe-S clusters essential for the activity of a specific subset of mitochondria proteins (Gelling et al., 2008; Johnson et al., 2005) but have not been directly implicated in heme biosynthesis.

In addition to predicting new components of the query pathway, expression screening also identifies the data sets in which coexpression occurs, thus suggesting biological contexts in which the pathway is active. For heme biosynthesis, the highest-scoring data set is a time course analysis of erythrocytes differentiating in vitro from primary human hematopoietic progenitor cells (Keller et al., 2006) (Figure 2A). Here, the eight heme biosynthesis enzymes are strongly induced at day 9, and at this time point, the candidates also reach peak expression, suggesting that they function during late erythrocyte differentiation, concurrent with hemoglobin synthesis. In contrast, early hematopoietic markers such as *CD34* and *GATA2* are expressed at early time points in this data set. In another high-scoring data set, we found upregulation of the candidates in Nix$^{-/-}$ mouse spleens (Figure 2B), which exhibit increased numbers of erythrocyte precursors due to a defect in mitochondria clearance during terminal erythrocyte differentiation (Diwan et al., 2007; Sandoval et al., 2008). Conversely, all candidates were downregulated when erythrocyte differentiation is abolished in Rb$^{-/-}$ fetal liver (Figure 2C) (Spike et al., 2007). Several multiple-tissue data sets were also high scoring due to strong expression in erythropoietic tissues such as bone marrow (Figure 2D). These contexts all reflect red blood cell biology, as expected. However, we also found regulation of the heme pathway in activated white blood cells and in some lymphomas, suggesting a previously unrecognized importance of heme biosynthesis in these contexts (Table S1 available online).

In Situ Expression Analysis of Five Candidate Genes in Zebrafish Embryos

To investigate the biological role of the five selected genes in red blood cell development, we used the zebrafish (*Danio rerio*), which serves as an excellent in vivo model system for studying hematological disorders (Shafizadeh and Paw, 2004). To identify zebrafish orthologs of the five candidates, we used reciprocal

Table 1. Top 30 Coexpressed Mitochondrial Genes Discovered by Expression Screening

Symbol	Description	Probability	Query	Heme	Fe-S	Follow-Up
UROD	uroporphyrinogen decarboxylase	1.00	X	X		
HMBS	hydroxymethylbilane synthase	1.00	X	X		
FECH	ferrochelatase (protoporphyria)	1.00	X	X		
ALAD	aminolevulinate, delta-, dehydratase	1.00	X	X		
GLRX5	glutaredoxin 5	1.00		X	X	
PPOX	protoporphyrinogen oxidase	1.00	X	X		
ALAS2	aminolevulinate, delta-, synthase 2	1.00	X	X		
ABCB6	ATP-binding cassette, subfamily B (MDR/TAP), member 6	1.00		X		
UROS	uroporphyrinogen III synthase (congenital erythropoietic porphyria)	0.99	X	X		
CPOX	coproporphyrinogen oxidase	0.99	X	X		
SLC25A37	solute carrier family 25, member 37	0.99		X		
PRDX2	peroxiredoxin 2	0.99				
ABCB10	ATP-binding cassette, subfamily B (MDR/TAP), member 10	0.99		X		
HAGH	hydroxyacylglutathione hydrolase	0.98				
TMEM14C	transmembrane protein 14C	0.97				X
SLC25A39	solute carrier family 25, member 39	0.96				X
TXNRD2	thioredoxin reductase 2	0.96				
NT5C3	5′-nucleotidase, cytosolic III	0.93				
NCOA4	nuclear receptor coactivator 4	0.85				
SLC22A4	solute carrier family 22 (organic cation transporter), member 4	0.81				X
UCP2	uncoupling protein 2 (mitochondrial, proton carrier)	0.80				
ISCA1	iron-sulfur cluster assembly 1 homolog (S. cerevisiae)	0.71			X	X
C10orf58	chromosome 10 open reading frame 58	0.68				
HK1	hexokinase 1	0.68				
ISCA2	iron-sulfur cluster assembly 2 homolog (S. cerevisiae)	0.62			X	
MCART1	mitochondrial carrier triple repeat 1	0.62				
FAHD1	fumarylacetoacetate hydrolase domain containing 1	0.59				
COX6B2	cytochrome c oxidase subunit VIb polypeptide 2 (testis)	0.55				
ATPIF1	ATPase inhibitory factor 1	0.49				
C1orf69	RIKEN cDNA A230051G13 gene	0.45			X	X

Query, genes used as input for screening; Heme, genes known to be required for functional heme biosynthesis; Fe-S, genes involved in iron-sulfur cluster assembly; Follow-up, candidates selected for further study.

protein-level BLAST. We were able to predict clear zebrafish orthologs for *SLC25A39*, *TMEM14C*, *C1orf69*, and *ISCA1*. However, mammalian *SLC22A4* exhibited close sequence similarity with zebrafish *slc22a4* and *slc22a5*, and a multiple alignment of these genes between mouse, human, and fish did not resolve the orthology (Figure S1). Therefore, we included both possible orthologs for functional follow-up.

Whole-mount in situ hybridization of zebrafish embryos at 24 hr postfertilization (hpf) showed clear localization of mRNA for *slc25a39*, *tmem14c*, and *c1orf69* (Figure 3) to the intermediate cell mass (ICM), the functional equivalent of mammalian yolk sac blood islands. Transcripts for *isca1*, *slc22a4*, and *slc22a5* did not show clear tissue-restricted expression in the developing zebrafish embryo (Figure 3); however, real-time quantitative RT-PCR analysis indicated very low levels of *slc22a4* and *slc22a5* mRNA in 24 hpf embryos (data not shown), possibly explaining absent staining in the ICM by the less-sensitive in situ hybridization method. Real-time qRT-PCR analysis of *isca1* mRNA, on the other hand, showed high overall expression

at 24 hpf (data not shown), indicating that *isca1* is not specific to the ICM. To clearly delineate the ICM, *slc4a1*, an erythroid-specific cytoskeletal protein (Paw et al., 2003), was included in the analysis (Figure 3A). We did not detect staining for any of these genes in zebrafish *cloche* (*clo*) mutants, which lack hematopoietic and vascular progenitors (Stainier et al., 1995), indicating specificity of the in situ hybridization results (*slc4a1*, Figure 3B; remaining genes, data not shown).

Knockdown in Zebrafish Results in Profound Anemia without Affecting Erythroid Specification

To evaluate a possible function in erythropoiesis, we disrupted mRNA expression of each candidate gene in developing zebrafish embryos using splice-blocking morpholino oligomers (Summerton and Weller, 1997). These knockdowns resulted in profound anemia, as indicated by the lack of hemoglobinized cells after staining the embryos with o-dianisidine (Figure 4), for all candidates except *slc22a4* (Figure 4D). Even at very high concentration, the *slc22a4*-targeting morpholino did not induce
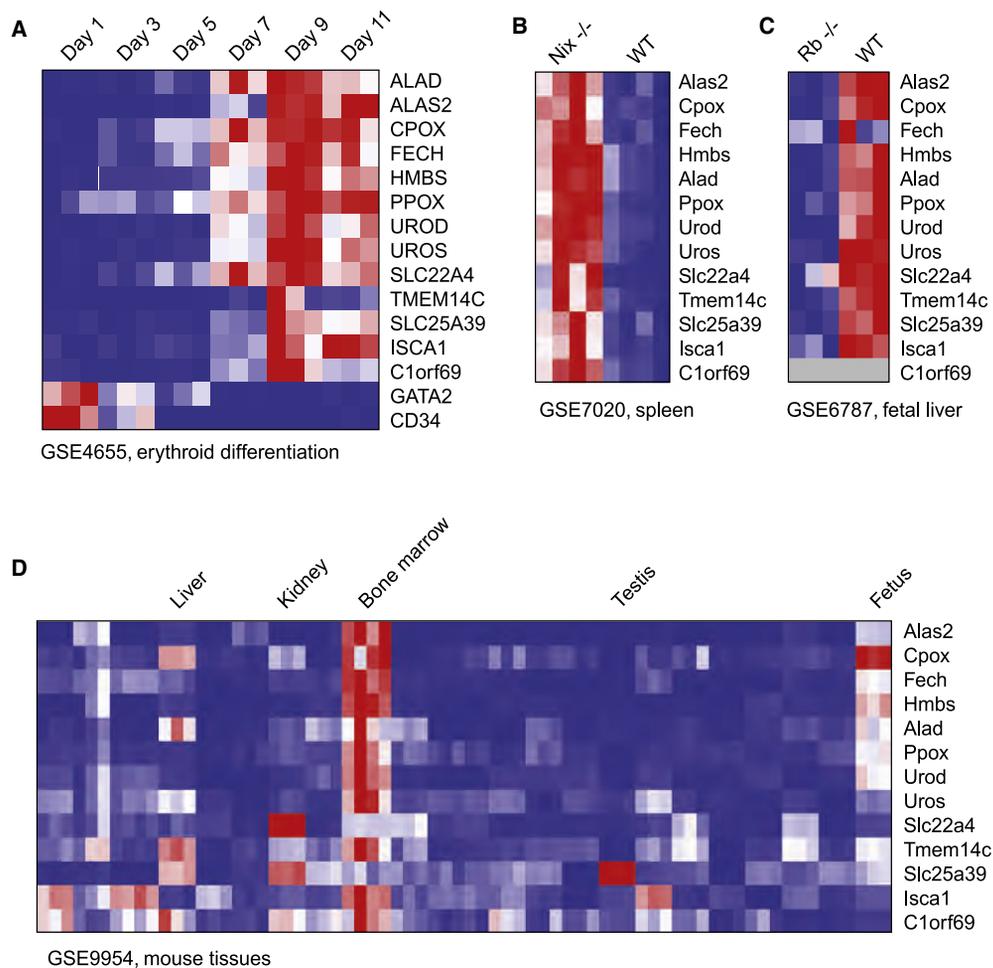
Figure 2. Microarray Data Sets in which the Heme Biosynthetic Pathway Is Regulated
(A) Time series gene expression of heme biosynthesis enzymes and five selected candidates (see text) during erythroid differentiation.
(B) Gene expression in Nix$^{-/-}$ and wild-type (WT) mouse spleen.
(C) Gene expression in Rb$^{-/-}$ and wild-type (WT) mouse fetal liver.
(D) Gene expression in a panel of mouse tissues.
Red indicates high expression; blue, low expression; gray, missing values. GSE, NCBI Gene Expression Omnibus accession number.

anemia. Therefore, the anemia resulting from *slc22a5* knockdown suggests that this gene and not *slc22a4* is the functional zebrafish ortholog of mammalian *SLC22A4*. A quantitative enumeration of the anemia in control and morphant embryos for each silenced gene is displayed in Figure S2. With the exception of anemia, the morphant embryos generally did not exhibit other gross developmental abnormalities at the chosen doses of morpholino. RT-PCR analysis of RNA isolated from the morphant embryos showed alternate mRNA species (eventually leading to nonsense-mediated mRNA decay) being generated for *slc25a39*, *slc22a4*, *slc22a5*, *tmem14c*, and *c1orf69*, but not for WT uninjected embryos (Figures 4B–F), demonstrating accurate gene targeting of the respective morpholinos. Off-target effects were excluded by normal RT-PCR products for the β-actin (*actb*) control. Because we could not detect alternate mRNA species in embryos injected with the *isca1*-targeted morpholino, we measured *isca1* mRNA expression by real-time qRT-PCR. Embryos injected with the *isca1* morpholino showed

a 3-fold downregulation compared to WT uninjected embryos (Figure 4G). Injection of a nonspecific standard control morpholino did not affect *isca1* mRNA expression levels (Figure 4G).

To show that the anemic phenotype observed by morpholino knockdown is not merely due to a lack of erythrocyte progenitors and is erythroid lineage specific, we stained morphant embryos for the erythroid lineage-specific gene αE3-globin (*hbae3*) at 24 and 48 hpf and for the myeloid lineage-specific gene myeloperoxidase (*mpo*) (Bennett et al., 2001) at 48 hpf by whole-mount in situ hybridization. The results indicate that expression of *mpo* and *hbae3* at 24 hpf was overall comparable to wild-type embryos, indicating that initial specification of erythropoiesis and myelopoiesis are not perturbed by deficiency of our candidate genes (Figure S3). A slight decrease in *hbae3* levels was observed at 48 hpf for all candidates except *slc22a4*. This probably reflects reduced viability of a number of erythroid cells, an expected consequence of silencing genes that perform important functions in erythroid cells. In summary, the loss of heme
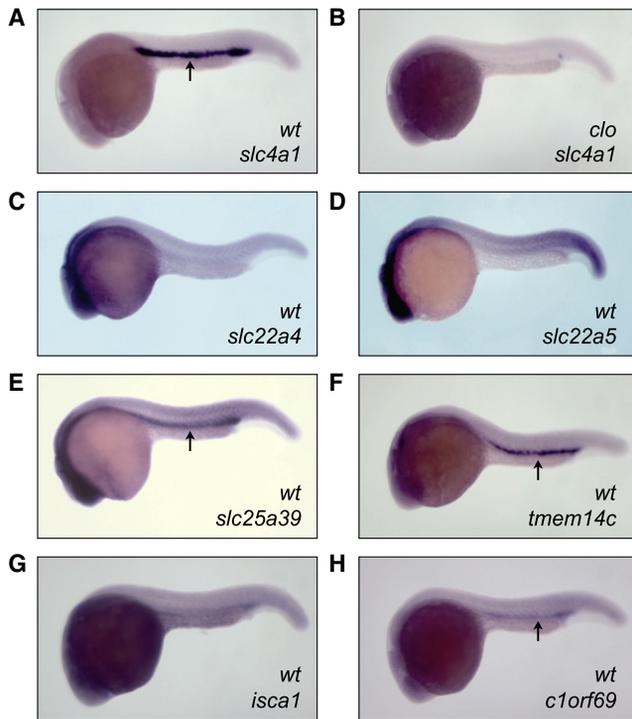
Figure 3. Expression of Candidate Genes in Zebrafish Blood Islands
Whole-embryo in situ hybridization was performed on embryos at 24 hpf.
(A) *slc4a1* was used as control to delineate the intermediate cell mass (ICM, indicated by arrows).
(B) *Cloche* (*clo*) embryos were used to show specificity of the hybridizations.
(C–H) Candidates identified in this study.

staining seen in Figure 4 is not due to defective erythroid lineage specification, and knockdowns do not affect other hematopoietic lineages such as myeloid cells, implicating erythroid-specific roles for the candidates.

Slc25a39 Is Highly Expressed in Mouse Hematopoietic Tissues

We chose to further investigate the function of *SLC25A39* because of its sequence homology to the *S. cerevisiae* gene *MTM1*, which has previously been implicated in iron homeostasis (Yang et al., 2006). To characterize its function in mammals, we first investigated the tissue distribution and developmental expression of murine *Slc25a39*. Northern blot analysis revealed abundant *Slc25a39* mRNA expression in the hematopoietic organs fetal liver, adult bone marrow, and spleen (Figure 5A). Significant mRNA expression was also observed in the testis and kidneys (Figure 5A). This expression profile is largely consistent with that observed in microarray data (Figure 2D). We also found that *Slc25a39* is highly expressed in primitive mouse erythroblasts that fill yolk sac blood islands at early somite pair stages (Figure 5B) and in fetal liver (midgestation at day E12.5), the site of definitive erythropoiesis (Figures 5C and 5D). This expression pattern is concordant with *slc25a39* staining in the zebrafish ICM and suggests that this gene functions in both primitive and definitive erythropoiesis in mammals.

Slc25a39 Is Required for Heme Synthesis, but Silencing Does Not Cause Porphyria

The reduced number of heme-positive cells seen in zebrafish *slc25a39* knockdowns could be caused by a defect in mitochondrial iron availability. To address this issue and investigate the biochemical role of *Slc25a39* in more detail, we labeled differentiating wild-type and *Slc25a39* siRNA-treated mouse erythroleukemia (MEL) cells with ^{59}Fe-saturated transferrin and assayed for ^{59}Fe incorporation into heme. We confirmed effective silencing of *Slc25a39* at the protein level by using western analysis (Figure 5E). Wild-type cells treated with nonspecific siRNA oligos efficiently incorporated ^{59}Fe into heme; however, *Slc25a39*-silenced cells showed a 4-fold reduction in ^{59}Fe-labeled heme, whereas total mitochondrial ^{59}Fe remained unaffected, thus excluding its function as a mitochondrial iron importer (Figure 5F). As a positive control, we also performed siRNA knockdown of the iron transporter *Slc25a37* (Shaw et al., 2006a), which resulted in marked reduction of total mitochondrial ^{59}Fe as well as heme incorporation of ^{59}Fe (Figure 5F). Simultaneous silencing of *Slc25a39* and *Slc25a37* did not affect mitochondrial iron content or heme formation more than silencing *Slc25a37* alone, indicating that *Slc25a37* is epistatic to *Slc25a39* for mitochondrial iron import. These data show that *Slc25a39* is essential for heme biosynthesis in mammals.

To further delineate the role of *SLC25A39* in heme biosynthesis, we asked whether its loss in zebrafish embryos causes a porphyric phenotype. Embryos injected with a morpholino targeting ferrochelatase clearly exhibited circulating, porphyric red blood cells (Figure 5H), but wild-type embryos and embryos injected with a morpholino targeting *slc25a39* did not (Figures 5G and 5I). Because defects in any of the terminal steps of heme biosynthesis cause accumulation of porphyrin intermediates, this result suggests that *SLC25A39* is involved in the early steps of heme synthesis or in the regulation of ALA synthase function.

Vertebrate *SLC25A39* Complements Mitochondrial Iron Homeostasis Defects in the Yeast *mtm1Δ* Mutant

SLC25A39 has clear sequence homology to the *S. cerevisiae* gene *MTM1*, for which a deletion strain *mtm1Δ* has been characterized that exhibits altered iron homeostasis. Loss of *MTM1* in yeast alters mitochondrial iron bioavailability such that iron gains access to the catalytic site of manganese superoxide dismutase 2 (Sod2p), thereby inactivating the enzyme (Yang et al., 2006). *MTM1* also genetically interacts with the yeast mitochondrial iron importers *MRS3* and *MRS4*, which are orthologs of the human *SLC25A37* (Yang et al., 2006). In addition, *mtm1Δ* mutants exhibit loss of mitochondrial DNA, elevations in Cu/Zn Sod1p activity, and an increased level of the mitochondrial Isu1p/Isu2p proteins needed for Fe-S cluster biogenesis (Luk et al., 2003; Yang et al., 2006; Naranuntarat et al., 2009). We expressed zebrafish *slc25a39* or mouse *Slc25a39* in yeast *mtm1Δ* mutants and found that these genes complement low-Sod2p and high-Sod1p activity, as well as the elevated protein levels of Isu1/2 (Figures 6A and 6B). This complementation was reversed upon subsequent shedding of the plasmid-derived clones with 5-FOA treatment, showing specificity of the assay (Figures 6A and 6B). We also observed that expression of zebrafish *slc25a39* protected against loss of mitochondrial DNA (and concomitant loss of genes important for mitochondrial
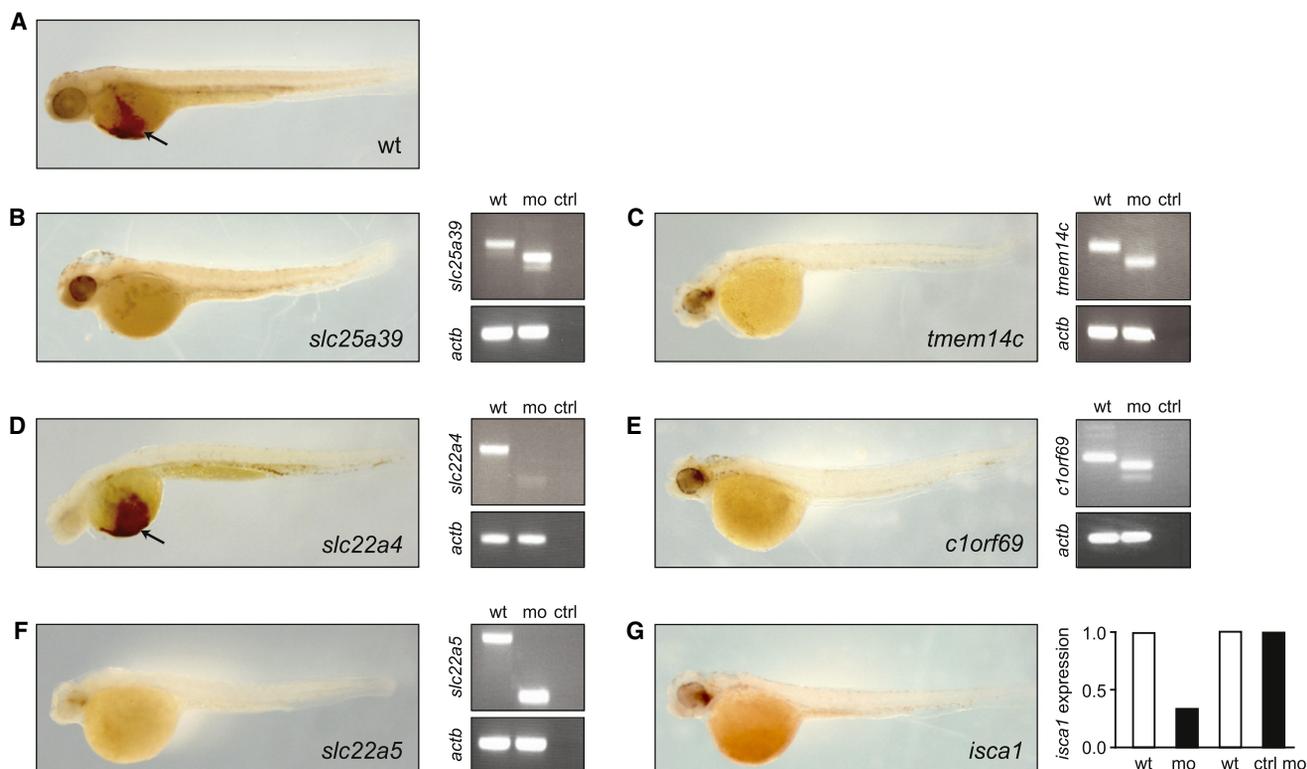
Figure 4. Morpholino Knockdown of Candidate Genes in Zebrafish Results in Profound Anemia
WT zebrafish embryos were injected at the one-cell stage with the respective morpholinos and stained at 48 hpf with *o*-dianisidine to detect hemoglobinized cells. (A) Uninjected (WT) embryos show normal hemoglobinization as indicated by dark brown staining on the yolk sac (arrow).
(B–G) Morpholino-injected embryos. Accurate morpholino gene targeting was verified by RT-PCR (*slc25a39*, *slc22a4*, *slc22a5*, *tmem14c*, and *c1orf69*) or real-time quantitative RT-PCR (*isca1*) on cDNA from uninjected (WT) or morpholino-injected (mo) embryos. β-actin (*actb*) was used as a control for off-target effects in the RT-PCR. For RT-PCR, (ctrl) indicates no cDNA template control. For real-time quantitative RT-PCR, (ctrl mo) indicates embryos injected with a standard control morpholino.

respiration) upon subsequent deletion of *MTM1*, as shown by a growth assay on nonfermentable carbon sources (Figure 6C). We conclude that *SLC25A39* is the functional vertebrate ortholog of yeast *MTM1*, supporting an important role for this gene in iron homeostasis.

DISCUSSION

Expression screening (Figure 1) is based on the simple principle that genes exhibiting a consistent correlation of mRNA levels across multiple experiments are more likely to be functionally related. We applied this method to the heme biosynthesis pathway and, as proof of principle, recovered four genes recently implicated in heme biosynthesis (*GLRX5*, *ABCB10*, *ABCB6*, and *SLC25A37*) among the top five predictions. This indicates high specificity of our expression screening predictions. In addition, a number of genes previously not associated with heme biosynthesis and mitochondrial iron homeostasis were identified. In some cases, their function was completely unknown prior to this study, whereas others, such as *ISCA1*, have been studied intensively but have not been linked to heme synthesis before. Remarkably, all five genes selected for follow-up studies resulted in an anemic phenotype when silenced in zebrafish embryos. We chose to further focus our

efforts on characterizing *SLC25A39*, and our data support an important role for this mitochondrial solute carrier in mammalian heme synthesis. These results warrant further studies of the remaining high-scoring candidates (Table 1).

Not all genes that showed strong coexpression in the screen are likely to be directly involved in heme biosynthesis. Some are presumably merely red blood cell specific, which is reasonable given that our screen was largely driven by erythrocyte gene expression. In this category, we find hexokinase 1 (*HK1*), which catalyzes the initial step in erythrocyte glycolysis, and glyoxalase II (*HAGH*), which is involved in synthesis of the antioxidant glutathione. We also detected several proteins thought to participate in erythrocyte oxidant defense, including *PRDX2* (Low et al., 2007) and *TXNRD2*. In addition, we identified *C10orf58*, an uncharacterized protein structurally similar to the thioredoxins, which could represent a hitherto unknown component of antioxidant defense.

Our large-scale computational analysis uncovered strong coexpression between heme biosynthesis and the Fe-S cluster assembly proteins *ISCA1*, *ISCA2*, and *C1orf69*. A functional link between these two processes was recently discovered in zebrafish erythrocytes, in which defects in the Fe-S cluster assembly protein *GLRX5* disrupt heme synthesis by inhibiting translation of *ALAS2* in erythrocytes through IRP1 (Wingert
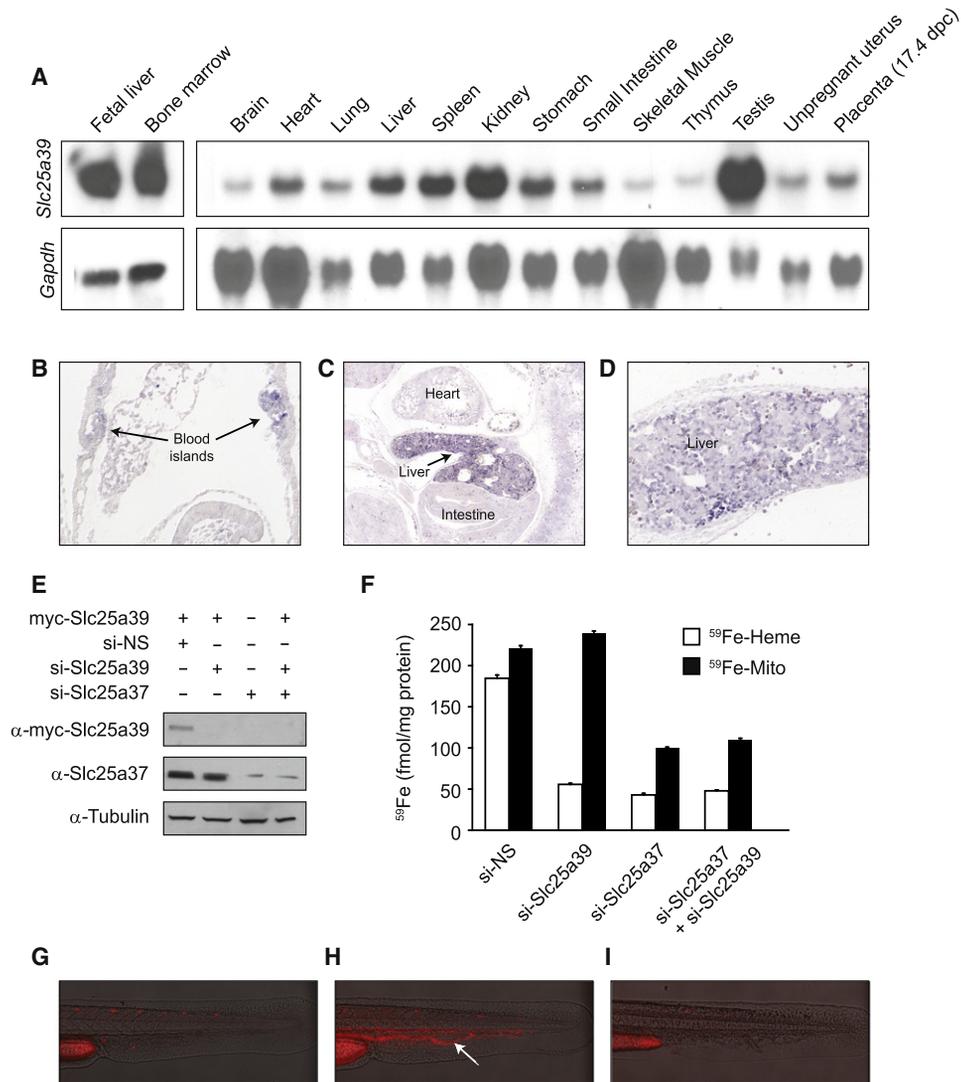
Figure 5. Mouse *Slc25a39* Is Expressed in Hematopoietic Tissues and Is Important for Heme Biosynthesis
(A) Mouse tissue northern blot analysis of *Slc25a39* expression.
(B) Mouse *Slc25a39* transcripts are localized to blood islands of the yolk sac at early somite stages (E8.5, arrows).
(C and D) *Slc25a39* transcripts accumulate most abundantly in the liver, where expression is heterogeneous (E12.5).
(E and F) MEL cells were differentiated for 2 days in media containing 1.5% DMSO prior to (E) transient transfection with myc-tagged *Slc25a39* or (F) silencing of *Slc25a39* (si-Slc25a39) and/or *Slc25a37* (si-Slc25a37) using siRNA oligos. Assays were performed after 2 additional days of differentiation. si-NS indicates silencing using nonspecific control oligos.
(E) Representative western blot using anti-myc (α-myc-Slc25a39) and anti-Slc25a37 antibodies. Equal loading was verified by anti-tubulin.
(F) MEL cells were metabolically labeled with ^{59}Fe conjugated to transferrin, and total mitochondrial iron (^{59}Fe-Mito) and iron in heme (^{59}Fe-Heme) were determined. Results shown are from two independent experiments assayed in duplicate; error bars denote standard deviation.
(G–I) Representative photos of (G) an uninjected, wild-type control zebrafish embryo, (H) a zebrafish embryo injected with a *ferrochelatase*-specific morpholino, or (I) a zebrafish embryo injected with a *slc25a39*-specific morpholino. Arrow indicates porphyric red blood cells in circulation.

et al., 2005). This regulatory mechanism is thought to act as a cellular iron sensor that prevents synthesis of the toxic porphyrins when iron is scarce. However, there are other plausible reasons for synchronizing Fe-S cluster assembly with heme synthesis. For example, both heme and Fe-S clusters serve as cofactors in electron-transferring proteins such as those in the respiratory chain. An Fe-S cluster is also required by mammalian ferrochelatase, which catalyzes the final step of heme synthesis. Moreover, the three Fe-S cluster synthesis proteins

identified in our screen (*ISCA1*, *ISCA2*, and *C1orf69*) appear to specialize in assembling Fe-S clusters on a subset of mitochondrial enzymes, including the citric acid cycle enzyme aconitase and lipoic acid synthetase, which produces an essential cofactor for the pyruvate dehydrogenase complex (Gelling et al., 2008; Lill and Mühlenhoff, 2008). Impaired assembly of Fe-S clusters on these enzymes could hamper the production of succinyl-CoA, which is required in vast amounts for erythroid heme synthesis (Figure 1A; Shemin et al., 1955). Further
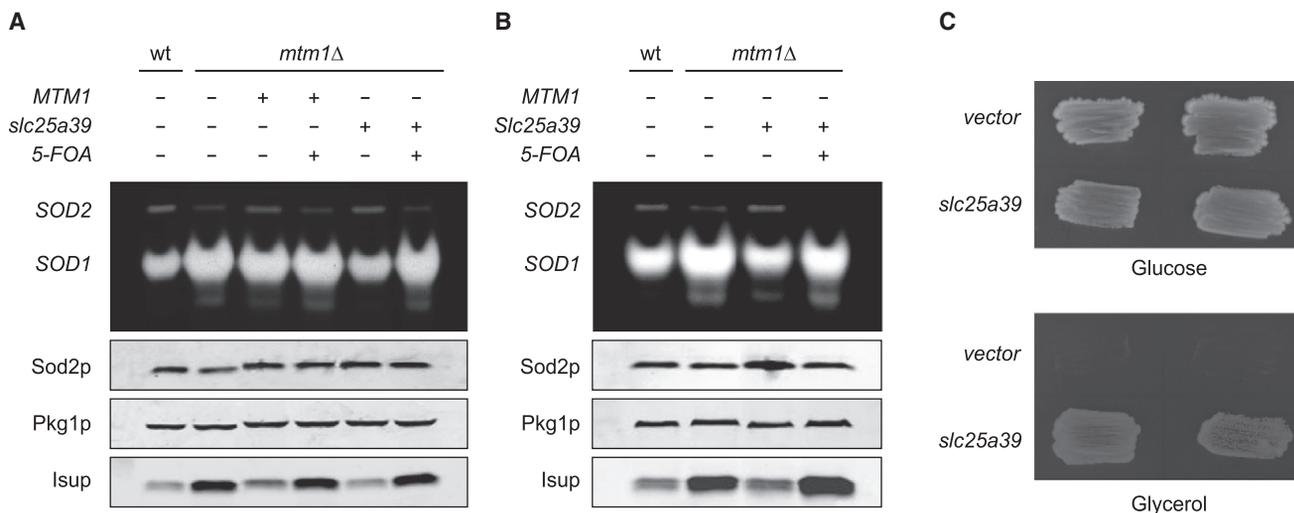
Figure 6. Vertebrate *SLC25A39* Is the Ortholog of Yeast *MTM1* and Is Involved in Mitochondrial Iron Homeostasis
(A and B) *mtm1Δ* strains were transformed with *URA3*-based plasmids for expressing (A and B) *S. cerevisiae MTM1*, (A) zebrafish *slc25a39*, or (B) mouse *Slc25a39*. 5-FOA indicates transformants induced to shed the plasmids by growth on 5-fluoroorotic acid. Whole-cell lysates of the transformants, 5-FOA derivatives, and the parental WT and *mtm1Δ* cells were subjected to (top) native gel electrophoresis and NBT staining for SOD (SOD2 and SOD1) activity and (bottom) to SDS-PAGE and immunoblotting for Sod2p, Pgk1 (loading control), and Isup (sum of Isu1p and Isu2p).
(C) WT strain transformed with either empty pRS426-ADH vector or zebrafish slc25A39 was subjected to *MTM1* deletion and tested for mitochondrial DNA function by growth on fermentable (glucose) versus nonfermentable (glycerol) carbon sources.
Results shown represent two independent colonies.

investigation is needed to determine which of these, or other, hypotheses are correct.

At the outset, one of this study's goals was to identify transporters responsible for trafficking heme precursors between the mitochondrial and cytosolic compartments. Expression screening implicated a handful of mitochondrial proteins with transmembrane domains that might be candidates for such transporters. One of these is the mitochondrial solute carrier *SLC22A4*. This gene is highly homologous to the carnitine transporter *SLC22A5* (*OCTN2*) but has low affinity for carnitine and does not rescue carnitine deficiency in mice (Zhu et al., 2000). *SLC22A4* has been suggested to protect red blood cells from oxidative stress (Grundemann et al., 2005), and a previous study found that terminal differentiation of MEL cells is disrupted upon *SLC22A4* depletion, although the cause of this is unclear (Nakamura et al., 2007). The protein is present in both the mitochondrial and plasma membranes (Lamhonwah and Tein, 2006). We also identified *TMEM14C*, a short mitochondrial transmembrane protein (112 amino acids). This gene is found only in vertebrate animals; it exhibits strong expression in zebrafish ICM and appears essential for functional heme biosynthesis in erythrocytes, making this a strong candidate for further studies. An additional high-scoring gene is *MCART1*, also a mitochondrial solute carrier. Its role in erythrocyte biology remains to be established.

In the current study, we chose to focus our efforts on the solute carrier *SLC25A39*. This gene localizes to the mitochondrial membrane (Luk et al., 2003; Yu et al., 2001), and we demonstrate that it is the functional vertebrate ortholog of yeast *MTM1*. *MTM1* was previously described as a manganese transporter (Luk et al., 2003), but *mtm1Δ* mutants do not show altered mitochondrial manganese levels, and more recent data suggest that its primary

role is in mitochondrial iron homeostasis (Luk et al., 2003). Deletion of *MTM1* causes mitochondrial iron overload (Yang et al., 2006) and upregulation of the Fe-S scaffold proteins Isu1 and Isu2 (Naranuntarat et al., 2009), phenotypes that we found to be complemented by vertebrate *SLC25A39*. Here, we show that *slc25a39* is required for heme synthesis in zebrafish. Furthermore, our data in MEL cells demonstrate that mouse *Slc25a39* is not an iron transporter, given that mitochondrial iron levels were unaffected when *Slc25a39* expression was silenced by siRNA. However, silencing of *Slc25a39* did affect iron incorporation into heme to an extent similar to that of *Slc25a37*, the principal mitochondrial iron importer in erythroid cells (Shaw et al., 2006a).

Based on our data in MEL cells, silencing *SLC25A39* either impairs incorporation of iron into PPIX by ferrochelatase or inhibits PPIX synthesis altogether; however, morpholino knockdown of *slc25a39* in zebrafish did not result in a porphyric phenotype, arguing against a direct participation of *SLC25A39* in the terminal steps of protoporphyrin synthesis. Thus, our data suggest a role for SLC25A39 either in early heme synthesis or in its regulation via ALA synthase. In vertebrate erythrocytes, availability of Fe-S clusters regulates ALAS2 through IRP1, demonstrated by recent work focusing on the zebrafish mutant *shiraz* (Wingert et al., 2005). This mutant harbored mutations in the Fe-S cluster enzyme *grx5*, which abolished heme biosynthesis. Interestingly, the observed phenotypic consequences of defects in *GLRX5* and *SLC25A39* are strikingly similar in both yeast and vertebrates; in zebrafish, neither defects in *slc25a39* nor in *grx5* result in porphyria (Figure 5; Wingert et al., 2005), and yeast *mtm1Δ* or *grx5Δ* cells both accumulate mitochondrial iron (Yang et al., 2006) and exhibit a marked increase in the Fe-S scaffold proteins Isu1/Isu2 (Figure 6; Bellí et al.,

2004). In general, defects in Fe-S cluster assembly in yeast result in mitochondrial iron overload, whereas heme deficiency due to dysfunctional ALA synthase does not (Crisp et al., 2003). Based on our and previously published observations, we hypothesize that vertebrate *SLC25A39* may be involved in Fe-S cluster synthesis and that the observed effects on heme synthesis (Figures 4B and 5F) might be mediated through IRP1, analogous to what has been described for *GLRX5* (Wingert et al., 2005), though future experiments will be required to critically test this hypothesis.

In summary, this study demonstrates that large-scale integration of gene expression data has the potential to identify additional components of partially known, transcriptionally regulated pathways with high precision. Our computational analysis and follow-up studies have identified and confirmed roles for five mitochondrial proteins in heme biosynthesis; revealed tightly coordinated expression of the iron sulfur cluster assembly and heme biosynthesis pathways in maturing erythrocytes; and specifically predicted a primary function for *SLC25A39* in Fe-S cluster assembly, which is required to maintain functional heme biosynthesis in developing erythrocytes. While the precise molecular function of this and other proteins identified herein remains to be addressed in full, our findings open up new avenues of research into erythrocyte biology and provide candidate genes for human hematological disorders.

EXPERIMENTAL PROCEDURES

Data Sets

All microarray data sets for five Affymetrix platforms (human U133A, U133+; mouse U74Av2, M430, and M430A) containing at least six arrays were downloaded from the NCBI Gene Expression Omnibus (GEO) (Barrett et al., 2007) during March 2008. Overlapping data sets were merged, resulting in 1426 distinct data sets. We used the signal-level data provided in GEO matrix files. Signal values were unlogged if necessary and normalized separately for each data set by scaling each array to its 2% trimmed mean. To establish a unique identifier per gene across species and platforms, we first mapped Affymetrix probesets to NCBI Gene IDs as previously described (Dai et al., 2005) and then mapped these to NCBI Homologene identifiers (Sayers et al., 2009). The set of 1097 genes encoding mitochondrial proteins was defined as previously described (Pagliarini et al., 2008) and mapped to Homologene identifiers, resulting in 1032 genes with homology between human and mouse.

Expression Screening

In brief, expression screening was performed as follows; the full details of the computational algorithm are described elsewhere (Baughman et al., 2009). We first treated each of the five microarray platforms separately. Affymetrix probesets for the eight heme biosynthesis enzymes were chosen manually by sequence matching to RefSeq transcript models. To avoid confounding the differently regulated liver and erythrocyte heme synthesis pathways, we included only the erythrocyte-specific form *ALAS2* for ALA synthase. For each data set, we calculated the GSEA-P enrichment score (Subramanian et al., 2005) between the heme biosynthesis probesets (the query pathway) and all other probesets matching the mitochondrial genes, using the Pearson correlation coefficient as the base measure. We repeated this procedure with arrays randomly permuted 100,000 times to generate a null distribution of enrichment scores. Global false discovery rate (FDR) estimation was then performed as previously described (Efron, 2007; Subramanian et al., 2005), and the coexpression probability q_{gd} (Figure 1A) was defined as 1 – FDR of probeset g in data set d. Data sets' weights w_d were defined as the average of q_{gd} with g ranging over the heme biosynthesis probesets. For each probeset, we integrated the false discovery rates from all data sets by using a robust Bayesian meta-analysis method (Genest and Schervish, 1985) to obtain the final probability p_g. Finally, we selected the best-scoring probeset for each

Homologene identifier and repeated this procedure across all platforms to obtain a unique p_g for each gene g with homology between mouse and human.

cDNA Clones

The cDNA clones from mouse and zebrafish for the candidate genes were obtained from Open Biosystems. The zebrafish cDNA clone for *slc22a5* was isolated by RT-PCR using primers based on the sequence in the GenBank database (XM_001340800) and total RNA from wild-type embryos at 19 hpf. GenBank accession numbers are as follows: Zebrafish clones for *slc25a39* (NM_200486), *slc22a5* (XM_001340800), *slc22a4* (NM_200849), *isca1* (NM_001025178), *c1orf69* (NM_001076635), and *tmem14c* (NM_001045438); mouse clones for *Slc25a39* (NM_026542), *Slc22a4* (NM_019687), *Isca1* (NM_026921), *C1orf69* (NM_173785), and *Tmem14c* (NM_025387).

Zebrafish Animal Husbandry

Standard AB and *cloche* (clo[m39]) strains were used in our studies and were raised in compliance with IACUC regulations.

Zebrafish In Situ Hybridization

Digoxigenin-labeled probe synthesis and whole-mount in situ hybridization was performed as described (Shaw et al., 2006a). For expression analysis of *slc22a4*, *slc22a5*, *slc25a39*, *c1orf69*, *isca1*, *tmem14c*, and *slc4a1*, 24 hpf embryos from matings between heterozygous *cloche* zebrafish were used. Myeloperoxidase and αE3-globin (*hbae3*) expression was determined in morpholino-injected AB wild-type embryos fixed at 24 and 48 hpf.

Morpholino Injections

Splice-junction-targeting morpholinos were ordered from Gene Tools (for sequences, see Table S2). AB wild-type embryos were injected at the one-cell stage and stained with *o*-dianisidine at 48 hpf as described (Shaw et al., 2006a). The injected morpholino concentrations ranged from 0.4 to 0.9 mM. The ferrochelatase-specific morpholino was as described (Wingert et al., 2005). Zebrafish pictures were taken with a Nikon Eclipse TE2000-E microscope and by using MetaMorph software.

RNA Isolation, cDNA Synthesis, and Real-Time PCR

Thirty control AB wild-type and morpholino-injected embryos were collected at 24 hpf, and RNA was isolated using TriZol Reagent (Invitrogen) and genomic DNA Eliminator columns (QIAGEN). RNA integrity was assessed on a 2% agarose gel, and yield was determined on a Spectrophotometer (Beckman). The First Strand cDNA Synthesis Kit (Roche) was used to generate cDNA from one microgram total RNA. Primer sequences for the detection of aberrantly spliced mRNA species are in Table S3. Real-time PCR was performed on an iQ5 Real-Time PCR Detection System (BIO-RAD). TaqMan Gene Expression Assays were obtained from Applied Biosystems. Samples were analyzed in triplicate, and normalized gene expression was calculated by using the $2^{-\Delta\Delta Ct}$ method (Schmittgen and Livak, 2008).

Mouse Tissue Northern Blots

The multiple tissue northern blot was obtained from Seegene. Ten micrograms of total RNA from mouse adult bone marrow and fetal liver were subjected to northern analysis. The nylon blots were serially hybridized with ^{32}P-labeled mouse *Slc25a39* and *Gapdh* probes by using standard procedures.

Mouse In Situ Hybridization

Nonradioactive in situ hybridization was performed by using antisense digoxigenin-UTP-labeled RNA probes (Roche). Procedures were essentially as described (Palis and Kingsley, 1995). In brief, five micron sections from paraformaldehyde-fixed, paraffin-embedded outbred mouse embryos were hybridized overnight at 52°C after proteinase K and acetic anhydride pretreatment. Posthybridization washes included RNase treatment. Alkaline-phosphatase-conjugated anti-digoxigenin antibodies were developed by using BM purple BCIP/NBT substrate (Roche).

siRNA Knockdown

siRNA oligos to *Slc25A39*, *Slc25A37*, and control oligos were purchased from Dharmacon. A myc-tagged cDNA for mouse *Slc25A39* was constructed in pCMV-Tag5 vector (Stratagene) and cotransfected into MEL cells using the

Amaxa nucleofection reagent and device. Western analysis with anti-myc and anti-tubulin antibodies was performed by using standard procedures. siRNA procedures in differentiating MEL cells and preparation of ^{59}Fe saturated transferrin were performed as described (Paradkar et al., 2009).

Yeast Complementation Analysis

The WT strain BY4741 and the isogenic MY019 (*mtm1Δ*) were as described (Yang et al., 2006). Strains were transformed by the lithium acetate procedure with *URA3* 2μ based vectors that either expressed *MTM1* from its native promoter (pLJ063) (Luk et al., 2003) or zebrafish slc25a39 and mouse Slc25A39. As needed, these transformants were induced to subsequently shed the *URA3*-based vectors by growth on medium containing 5-fluoroorotic acid (5-FOA) (Boeke et al., 1987). Cells were grown without shaking for 18–20 hr to a final OD$_{600}$ to midlog phase in SD (synthetic dextrose) medium (Sherman et al., 1978). The whole-cell lysates prepared by glass bead homogenization were analyzed for SOD activity by native gel electrophoresis and nitroblue tetrazolium (NBT) staining and for immunoblot analysis of yeast Sod2p (Luk et al., 2003), Pgk1p (Jensen et al., 2004), and total Isu1p and Isu2p using an anti-*E. coli* IscU antibody kindly provided by L. Vickery (Garland et al., 1999). To test for complementation of the *mtm1Δ* loss of mitochondrial DNA, WT cells transformed with either pRS426-ADH empty vector or with zSLC25A39 were subjected to a *MTM1* gene deletion using the *mtm1::LEU2* plasmid pVC257 (Luk et al., 2003). The resultant *mtm1::LEU2* derivatives were then tested for growth on enriched yeast extract peptone-based medium containing either fermentable (2% glucose) or nonfermentable (3% glycerol) carbon sources.

SUPPLEMENTAL DATA

Supplemental Data include three tables and three figures and can be found with this article online at http://www.cell.com/cell-metabolism/supplemental/S1550-4131(09)00196-X.

REFERENCES

Ajioka, R.S., Phillips, J.D., and Kushner, J.P. (2006). Biosynthesis of heme in mammals. Biochim. Biophys. Acta *1763*, 723–736.

Allikmets, R., Raskind, W.H., Hutchinson, A., Schueck, N.D., Dean, M., and Koeller, D.M. (1999). Mutation of a putative mitochondrial iron transporter gene (ABC7) in X-linked sideroblastic anemia and ataxia (XLSA/A). Hum. Mol. Genet. *8*, 743–749.

Barrett, T., Troup, D.B., Wilhite, S.E., Ledoux, P., Rudnev, D., Evangelista, C., Kim, I.F., Soboleva, A., Tomashevsky, M., and Edgar, R. (2007). NCBI GEO: mining tens of millions of expression profiles–database and tools update. Nucleic Acids Res. *35*, D760–D765.

Baughman, J.M., Nilsson, R., Gohil, V.M., Arlow, D.H., Gauhar, Z., and Mootha, V.K. (2009). A computational screen for regulators of oxidative phos-

phorylation implicates SLIRP in mitochondrial RNA homeostasis. PLoS Genetics. in press.

Bellí, G., Molina, M.M., García-Martinez, J., Pérez-Ortín, J.E., and Herrero, E. (2004). *Saccharomyces cerevisiae* glutaredoxin 5-deficient cells subjected to continuous oxidizing conditions are affected in the expression of specific sets of genes. J. Biol. Chem. *279*, 12386–12395.

Bennett, C.M., Kanki, J.P., Rhodes, J., Liu, T.X., Paw, B.H., Kieran, M.W., Langenau, D.M., Delahaye-Brown, A., Zon, L.I., Fleming, M.D., et al. (2001). Myelopoiesis in the zebrafish, Danio rerio. Blood *98*, 643–651.

Boeke, J.D., Trueheart, J., Natsoulis, G., and Fink, G.R. (1987). 5-Fluoroorotic acid as a selective agent in yeast molecular genetics. Methods Enzymol. *154*, 164–175.

Cahan, P., Rovegno, F., Mooney, D., Newman, J.C., St Laurent, G., III, and McCaffrey, T.A. (2007). Meta-analysis of microarray results: challenges, opportunities, and recommendations for standardization. Gene *401*, 12–18.

Camaschella, C., Campanella, A., De Falco, L., Boschetto, L., Merlini, R., Silvestri, L., Levi, S., and Iolascon, A. (2007). The human counterpart of zebrafish shiraz shows sideroblastic-like microcytic anemia and iron overload. Blood *110*, 1353–1358.

Cooperman, S.S., Meyron-Holtz, E.G., Olivierre-Wilson, H., Ghosh, M.C., McConnell, J.P., and Rouault, T.A. (2005). Microcytic anemia, erythropoietic protoporphyria, and neurodegeneration in mice with targeted deletion of iron-regulatory protein 2. Blood *106*, 1084–1091.

Cotter, P.D., Baumann, M., and Bishop, D.F. (1992). Enzymatic defect in "X-linked" sideroblastic anemia: molecular evidence for erythroid delta-aminolevulinate synthase deficiency. Proc. Natl. Acad. Sci. USA *89*, 4028–4032.

Crisp, R.J., Pollington, A., Galea, C., Jaron, S., Yamaguchi-Iwai, Y., and Kaplan, J. (2003). Inhibition of heme biosynthesis prevents transcription of iron uptake genes in yeast. J. Biol. Chem. *278*, 45499–45506.

Dai, M., Wang, P., Boyd, A.D., Kostov, G., Athey, B., Jones, E.G., Bunney, W.E., Myers, R.M., Speed, T.P., Akil, H., et al. (2005). Evolving gene/transcript definitions significantly alter the interpretation of GeneChip data. Nucleic Acids Res. *33*, e175.

Diwan, A., Koesters, A.G., Odley, A.M., Pushkaran, S., Baines, C.P., Spike, B.T., Daria, D., Jegga, A.G., Geiger, H., Aronow, B.J., et al. (2007). Unrestrained erythroblast development in Nix−/− mice reveals a mechanism for apoptotic modulation of erythropoiesis. Proc. Natl. Acad. Sci. USA *104*, 6794–6799.

Efron, B. (2007). Size, power and false discovery rates. Annals of Statistics *35*, 1351–1377.

Garland, S.A., Hoff, K., Vickery, L.E., and Culotta, V.C. (1999). Saccharomyces cerevisiae ISU1 and ISU2: members of a well-conserved gene family for iron-sulfur cluster assembly. J. Mol. Biol. *294*, 897–907.

Gelling, C., Dawes, I.W., Richhardt, N., Lill, R., and Mühlenhoff, U. (2008). Mitochondrial Iba57p is required for Fe/S cluster formation on aconitase and activation of radical SAM enzymes. Mol. Cell. Biol. *28*, 1851–1861.

Genest, C., and Schervish, M.J. (1985). Modeling expert judgements for Bayesian updating. The Annals of Statistics *13*, 1198–1212.

Grundemann, D., Harlfinger, S., Golz, S., Geerts, A., Lazar, A., Berkels, R., Jung, N., Rubbert, A., and Schomig, E. (2005). Discovery of the ergothioneine transporter. Proc. Natl. Acad. Sci. USA *102*, 5256–5261.

Guernsey, D.L., Jiang, H., Campagna, D.R., Evans, S.C., Ferguson, M., Kellogg, M.D., Lachance, M., Matsuoka, M., Nightingale, M., Rideout, A., et al. (2009). Mutations in mitochondrial carrier family gene SLC25A38 cause nonsyndromic autosomal recessive congenital sideroblastic anemia. Nat. Genet. *41*, 651–653.

Jensen, L.T., Sanchez, R.J., Srinivasan, C., Valentine, J.S., and Culotta, V.C. (2004). Mutations in Saccharomyces cerevisiae iron-sulfur cluster assembly genes and oxidative stress relevant to Cu, Zn superoxide dismutase. J. Biol. Chem. *279*, 29938–29943.

Johnson, D.C., Dean, D.R., Smith, A.D., and Johnson, M.K. (2005). Structure, function, and formation of biological iron-sulfur clusters. Annu. Rev. Biochem. *74*, 247–281.

Keller, M.A., Addya, S., Vadigepalli, R., Banini, B., Delgrosso, K., Huang, H., and Surrey, S. (2006). Transcriptional regulatory network analysis of developing human erythroid progenitors reveals patterns of coregulation and potential transcriptional regulators. Physiol. Genomics 28, 114–128.

Krishnamurthy, P.C., Du, G., Fukuda, Y., Sun, D., Sampath, J., Mercer, K.E., Wang, J., Sosa-Pineda, B., Murti, K.G., and Schuetz, J.D. (2006). Identification of a mammalian mitochondrial porphyrin transporter. Nature 443, 586–589.

Lamhonwah, A.M., and Tein, I. (2006). Novel localization of OCTN1, an organic cation/carnitine transporter, to mammalian mitochondria. Biochem. Biophys. Res. Commun. 345, 1315–1325.

Lange, H., Mühlenhoff, U., Denzel, M., Kispal, G., and Lill, R. (2004). The heme synthesis defect of mutants impaired in mitochondrial iron-sulfur protein biogenesis is caused by reversible inhibition of ferrochelatase. J. Biol. Chem. 279, 29101–29108.

Lill, R., and Mühlenhoff, U. (2008). Maturation of iron-sulfur proteins in eukaryotes: mechanisms, connected processes, and diseases. Annu. Rev. Biochem. 77, 669–700.

Low, F.M., Hampton, M.B., Peskin, A.V., and Winterbourn, C.C. (2007). Peroxiredoxin 2 functions as a noncatalytic scavenger of low-level hydrogen peroxide in the erythrocyte. Blood 109, 2611–2617.

Luk, E., Carroll, M., Baker, M., and Culotta, V.C. (2003). Manganese activation of superoxide dismutase 2 in Saccharomyces cerevisiae requires MTM1, a member of the mitochondrial carrier family. Proc. Natl. Acad. Sci. USA 100, 10353–10357.

May, B.K., Dogra, S.C., Sadlon, T.J., Bhasker, C.R., Cox, T.C., and Bottomley, S.S. (1995). Molecular regulation of heme biosynthesis in higher vertebrates. Prog. Nucleic Acid Res. Mol. Biol. 51, 1–51.

Muckenthaler, M.U., Galy, B., and Hentze, M.W. (2008). Systemic iron homeostasis and the iron-responsive element/iron-regulatory protein (IRE/IRP) regulatory network. Annu. Rev. Nutr. 28, 197–213.

Nakamura, T., Sugiura, S., Kobayashi, D., Yoshida, K., Yabuuchi, H., Aizawa, S., Maeda, T., and Tamai, I. (2007). Decreased proliferation and erythroid differentiation of K562 cells by siRNA-induced depression of OCTN1 (SLC22A4) transporter gene. Pharm. Res. 24, 1628–1635.

Naranuntarat, A., Jensen, L.T., Pazicni, S., Penner-Hahn, J.E., and Culotta, V.C. (2009). The interaction of mitochondrial iron with manganese superoxide dismutases. J. Biol. Chem. Published online June 27, 2009. 10.1074/jbc.M109.026773.

Pagliarini, D.J., Calvo, S.E., Chang, B., Sheth, S.A., Vafai, S.B., Ong, S.E., Walford, G.A., Sugiana, C., Boneh, A., Chen, W.K., et al. (2008). A mitochondrial protein compendium elucidates complex I disease biology. Cell 134, 112–123.

Palis, J., and Kingsley, P.D. (1995). Differential gene expression during early murine yolk sac development. Mol. Reprod. Dev. 42, 19–27.

Paradkar, P.N., Zumbrennen, K.B., Paw, B.H., Ward, D.M., and Kaplan, J. (2009). Regulation of mitochondrial iron import through differential turnover of mitoferrin1 and mitoferrin2. Mol. Cell. Biol. 29, 1007–1016.

Paw, B.H., Davidson, A.J., Zhou, Y., Li, R., Pratt, S.J., Lee, C., Trede, N.S., Brownlie, A., Donovan, A., Liao, E.C., et al. (2003). Cell-specific mitotic defect and dyserythropoiesis associated with erythroid band 3 deficiency. Nat. Genet. 34, 59–64.

Pondarre, C., Campagna, D.R., Antiochos, B., Sikorski, L., Mulhern, H., and Fleming, M.D. (2007). Abcb7, the gene responsible for X-linked sideroblastic anemia with ataxia, is essential for hematopoiesis. Blood 109, 3567–3569.

Ponka, P. (1997). Tissue-specific regulation of iron metabolism and heme synthesis: distinct control mechanisms in erythroid cells. Blood 89, 1–25.

Quackenbush, J. (2001). Computational analysis of microarray data. Nat. Rev. Genet. 2, 418–427.

Rouault, T.A. (2006). The role of iron regulatory proteins in mammalian iron homeostasis and disease. Nat. Chem. Biol. 2, 406–414.

Sandoval, H., Thiagarajan, P., Dasgupta, S.K., Schumacher, A., Prchal, J.T., Chen, M., and Wang, J. (2008). Essential role for Nix in autophagic maturation of erythroid cells. Nature 454, 232–235.

Sassa, S. (2006). Modern diagnosis and management of the porphyrias. Br. J. Haematol. 135, 281–292.

Sayers, E.W., Barrett, T., Benson, D.A., Bryant, S.H., Canese, K., Chetvernin, V., Church, D.M., DiCuccio, M., Edgar, R., Federhen, S., et al. (2009). Database resources of the National Center for Biotechnology Information. Nucleic Acids Res. 37, D5–D15.

Schmittgen, T.D., and Livak, K.J. (2008). Analyzing real-time PCR data by the comparative C(T) method. Nat. Protoc. 3, 1101–1108.

Shafizadeh, E., and Paw, B.H. (2004). Zebrafish as a model of human hematologic disorders. Curr. Opin. Hematol. 11, 255–261.

Shaw, G.C., Cope, J.J., Li, L., Corson, K., Hersey, C., Ackermann, G.E., Gwynn, B., Lambert, A.J., Wingert, R.A., Traver, D., et al. (2006a). Mitoferrin is essential for erythroid iron assimilation. Nature 440, 96–100.

Shaw, G.C., Langer, N.B., Wang, Y., Li, L., Kaplan, J., Bloomer, J.R., and Paw, B.H. (2006b). Abnormal expression of human mitoferrin (SLC25A37) is associated with a variant of erythropoietic protoporphyria. Blood 103, 6A.

Shemin, D., Russell, C.S., and Abramsky, T. (1955). The succinate-glycine cycle. I. The mechanism of pyrrole synthesis. J. Biol. Chem. 215, 613–626.

Sherman, F., Fink, G.R., and Lawrence, C.W. (1978). Methods in yeast genetics (Cold Spring Harbor, NY: Cold Spring Harbor Laboratory Press).

Shirihai, O.S., Gregory, T., Yu, C., Orkin, S.H., and Weiss, M.J. (2000). ABC-me: a novel mitochondrial transporter induced by GATA-1 during erythroid differentiation. EMBO J. 19, 2492–2502.

Spike, B.T., Dibling, B.C., and Macleod, K.F. (2007). Hypoxic stress underlies defects in erythroblast islands in the Rb-null mouse. Blood 110, 2173–2181.

Stainier, D.Y., Weinstein, B.M., Detrich, H.W., III, Zon, L.I., and Fishman, M.C. (1995). Cloche, an early acting zebrafish gene, is required by both the endothelial and hematopoietic lineages. Development 121, 3141–3150.

Subramanian, A., Tamayo, P., Mootha, V.K., Mukherjee, S., Ebert, B.L., Gillette, M.A., Paulovich, A., Pomeroy, S.L., Golub, T.R., Lander, E.S., et al. (2005). Gene set enrichment analysis: a knowledge-based approach for interpreting genome-wide expression profiles. Proc. Natl. Acad. Sci. USA 102, 15545–15550.

Summerton, J., and Weller, D. (1997). Morpholino antisense oligomers: design, preparation, and properties. Antisense Nucleic Acid Drug Dev. 7, 187–195.

Whatley, S.D., Ducamp, S., Gouya, L., Grandchamp, B., Beaumont, C., Badminton, M.N., Elder, G.H., Holme, S.A., Anstey, A.V., Parker, M., et al. (2008). C-terminal deletions in the ALAS2 gene lead to gain of function and cause X-linked dominant protoporphyria without anemia or iron overload. Am. J. Hum. Genet. 83, 408–414.

Wingert, R.A., Galloway, J.L., Barut, B., Foott, H., Fraenkel, P., Axe, J.L., Weber, G.J., Dooley, K., Davidson, A.J., Schmid, B., et al. (2005). Deficiency of glutaredoxin 5 reveals Fe-S clusters are required for vertebrate haem synthesis. Nature 436, 1035–1039.

Yang, M., Cobine, P.A., Molik, S., Naranuntarat, A., Lill, R., Winge, D.R., and Culotta, V.C. (2006). The effects of mitochondrial iron homeostasis on cofactor specificity of superoxide dismutase 2. EMBO J. 25, 1775–1783.

Yu, X.X., Lewin, D.A., Zhong, A., Brush, J., Schow, P.W., Sherwood, S.W., Pan, G., and Adams, S.H. (2001). Overexpression of the human 2-oxoglutarate carrier lowers mitochondrial membrane potential in HEK-293 cells: contrast with the unique cold-induced mitochondrial carrier CGI-69. Biochem. J. 353, 369–375.

Zhu, Y., Jong, M.C., Frazer, K.A., Gong, E., Krauss, R.M., Cheng, J.F., Boffelli, D., and Rubin, E.M. (2000). Genomic interval engineering of mice identifies a novel modulator of triglyceride production. Proc. Natl. Acad. Sci. USA 97, 1137–1142.